Haider Syed, Aftab (Orcid ID: 0000-0002-7072-1554)
Bougher Stephen, W. (Orcid ID: 0000-0002-4178-2729)

Effect of dust storm and GCR impact on the production rate of O_3^+ in MY 28 and MY 29: Modeling and SPICAM observation

S. A. Haider[1], Y. S. Siddhi[1,2], J. Masoom[1,2], S. Bougher[3]

[1]Planetary Sciences Division, Physical research Laboratory, Ahmedabad, India
[2]Research Scholar, Faculty of Science, Pacific Academy of Higher Education of Research University, Udaipur, India
[3]Climate and Space Sciences and Engineering, University of Michigan, Ann Arbor, USA

Abstract

We have developed a seasonally dependent energy loss model to calculate the zonally averaged production rates of O_3^+ due to impact of Galactic Cosmic Rays (GCR) in the dayside troposphere of Mars between solar longitudes (Ls) ~ 0° and 360° at low latitudes (2°N, 2°S, 25°N and 25°S), mid latitudes (45° and 45°S) and high latitudes (70°N and 70°S) in the Martian Year (MY) 28 and MY 29. We also represent the seasonal variability of zonally averaged ozone column density obtained from Mars Climate Database (MCD) [*Millour* et al., 2014] during the daytime. These results are compared with the daytime observations of column ozone made by Spectroscopy for the Investigation of the Characteristics of the Atmosphere of Mars (SPICAM) onboard Mars Express (MEX). At mid-to high latitudes ozone column density is maximum in northern winter and minimum in southern summer. At low-to-mid latitudes (2°N-S, 25°N-S and 45°N-S), the production rates of O_3^+ represent a broad peak between altitudes 26 km and 45 km in both hemispheres. The peak production rates are increasing up to Ls = 47.5° and then stabilized at about 2.5×10^{-8} cm^{-3} s^{-1}. At Ls $\geq$ 47.5° the peak production rate of O_3^+

This is the author manuscript accepted for publication and has undergone full peer review but has not been through the copyediting, typesetting, pagination and proofreading process, which may lead to differences between this version and the Version of Record. Please cite this article as doi: 10.1029/2018JA026200

This article is protected by copyright. All rights reserved.

Author Manuscript

starts decreasing until it disappeared after Ls = 127.5^o. A major dust storm occurred in MY 28 at Ls ~ 280^o in southern latitudes (~25^o-35^{o}S). During the dust storm period, dust opacity, ozone column density and O_3^+ production rate on the surface of Mars were increased by a factor of ~3.

1. Introduction

The O_3 molecule is formed from the product of O and O_2 by three body reaction using CO_2 as third body. It is destroyed by hydrogen radicals. An anti-correlation between the abundances of ozone and water vapor exist in the atmosphere of Mars [*Lefevre et al.*, 2008]. The neutral chemistry of O_3 has been discussed by several investigators in the Martian atmosphere [*Lefevre et al*., 2004, 2008; *Montmessin and Lefevre*, 2013]. They have reported that O_3 column density is maximum at high latitude and minimum at low latitude. The ion chemistry of O_3^+ is not understood globally in the lower ionosphere of Mars. Ozone is very important for the negative ion chemistry of Mars. It plays a very important role in the formation of the D layer of the ionosphere and also affects the atmospheric electricity on Mars [*Molina-Cuberos et al*., 2002; *Thomas and Gierasch, 1985*]. In the negative ion chemistry O^- is produced first by electron capture of O_3. Later three body reaction of CO_2 with O^- produces CO_3^-, which is associated with water and form a broad peak of water cluster ions $CO_3^-(H_2O)_n$ at about 30 km [*Molina-Cuberos et al*., 2002; *Haider et al*., 2007]. This peak was first reported by *Whitten et al.* [1971] as a D layer in the lower ionosphere of Mars. The D layer occurs

This article is protected by copyright. All rights reserved.

Author Manuscript

Author Manuscript

due to high efficiency of electron attachment to Ox molecules, which entails that the concentrations of negative ions are higher than that of electron below 30 km [*Haider et al.,* 2009].

In presence of dust storms the production of O_3 is more which produces more negative ions $CO_3^-(H_2O)_n$ and increased the D layer of the Mars' ionosphere. [cf. *Molina-Cuberos et al.,* 2006; *Michael et al.,* 2007; *Tolendo-Redondo et al.,* 2017]. During the dust storms dust aerosols are charged. The interaction of negative cluster ions $CO_3^-(H_2O)_n$ with positive charged aerosols reduced the D layer significantly [*Haider et al.,* 2010]. Therefore D layer disappeared for few weeks until the dust storm settles down to the normal condition. Thus, the electron capture of O_3 is initially creating more negative cluster ions $CO_3^-(H_2O)_n$ in presence of dust storms when the concentrations of O_3 were increased significantly. Later the productions of $CO_3^-(H_2O)_n$ were destroyed due to their attachment with the positive charged aerosols.

Several dust storms have been observed on Mars in MY10, MY13, MY25 and MY28 [*Martin*, 1984, 1995; *Smith et al*., 2013; *Montabone et al*., 2015]. The SPICAM spectrometer onboard MEX has provided continuous observations of UV dust opacity [*Montmessin et al.,* 2017]. It has also observed column O_3 at different Ls, latitude and longitude [*Bertaux et al.,* 2006]. The orbit of MEX does not change significantly with longitude [*Smith et al*, 2013]. Therefore we have averaged SPICAM observations over longitude for each Ls and latitude. These observations are compared with the zonally

This article is protected by copyright. All rights reserved.

Author Manuscript

averaged ozone column densities obtained from MCD (Mars Climate database) (website:http://www-mars.lmd.jussieu.fr) [*Millour et al.*, 2014].

In the present paper we have also calculated annual seasonal dependence of the production rates of O_3^+ using energy loss model [*Haider et al.*, 2007, 2008, 2009, 2015] due to impact of GCR in the dayside troposphere of Mars in presence and absence of dust storm during MY28 and MY29 respectively. These production rates can be used in future for the global modeling of the D region ionosphere of Mars. It is found that the production rates of O_3^+ are changing with season and produce a broad peak at low latitude between altitudes 30 km and 40 km. The peak production rates of O_3^+ increases up to $Ls=47.5^o$ while it decreases between $Ls=47.5^o$ and $Ls=127.5^o$. The O_3^+ production layer disappeared after $Ls=127.5^o$. The production rates of O_3^+ were also enhanced significantly on the surface of Mars in MY28 during dust storm period when the optical depth of dust increased up to 3.

2. Motivation and Objectives

The nighttime measurements of ozone were carried out by SPICAM using the stellar occultation method [*Montmessin and Lefevre*, 2013]. This measurement cannot provide altitude profiles of ozone in the daytime atmosphere at altitude ≤ 60-80 km where star signals are very weak [*Bertaux et al.*, 2006]. SPICAM also measured seasonal variability of ozone column abundance in the dayside atmosphere of Mars at different latitudes and longitudes. The column density of ozone varies strongly with latitudes and

This article is protected by copyright. All rights reserved.

Author Manuscript

seasons. This is due to the fact that solar UV radiation is highest on average in the tropics and the large scale air circulation in the troposphere slowly transports tropical ozone toward the pole. In presence of dust storm of MY28 ozone increases due to prominent drop of water abundance near the surface [*Montmessin et al.*, 2017]. This sudden decrease of water is also reported by Compact Reconnaissance Imaging Spectrometer (CRISM) during the dust storm of MY28 [*Smith,* 2009].

The seasonal cycle of Mars is dominated by a strong and asymmetric Hadley cell, extending between north and south mid-latitudes producing trade winds and allowing cross equatorial transport of dust and trace gases. The seasonal and latitudinal variability of ozone in MY 28 (in the presence of a dust storm) and MY 29 (in the absence of a dust storm) are not studied in detail during the daytime atmosphere of Mars. We have extended energy loss model of *Haider et al.* [2009] to calculate the production rates of O_3^+ in presence and absence of dust storms between Ls = 0^o and 360^o at low latitudes (2^oN, 2^oS, 25^oN and 25^oS), mid latitudes (45^oN and 45^oS) and high latitudes (70^oN and 70^oS). The three main objectives of this paper are given below:

(1) The column **of** ozone is observed in the daytime from the SPICAM instrument. We have compared seasonal variability of the ozone column observed by SPICAM with the model results of MCD in MY 28 and MY 29.

(2) The annual variability of the production rate of O_3^+ is not measured or estimated in the daytime atmosphere of Mars. We have simulated altitude profiles of the

This article is protected by copyright. All rights reserved.

Author Manuscript

production rate of O_3^+ during the daytime at different seasons and latitudes in MY 28 and MY 29.

(3) The effect of a dust storm is a key problem in the lower atmosphere of Mars. We have studied seasonal and latitudinal dependence of the production rates of O_3^+ in presence and absence of a dust storm corresponding to MY 28 and MY 29 respectively.

3. Model

3.1 GCR Impact Ionization Rate

The impact of primary cosmic rays, mainly protons and particles onto the Martian atmospheric gases produce protons, neutrons, and pions. Fast secondary nucleons can gain enough energy to increase the production of particles by neutral collisions. Neutral pions quickly decay to gamma rays, and their contribution to the energy deposition is very important in the lower atmosphere of Mars. At high altitude the maximum ion production rates are due to protons. Charged pions do not decay to muons before reaching the ground**.** Therefore, the muon energy is mainly transferred to the surface of Mars [*Molina-Cuberos* et al., 2002]. *Haider* et al. [2007, 2009] used energy loss method and developed a GCR impact ionization model to calculate altitude profiles of ion production rates in the lower ionosphere of Mars. In this model the effects of seasonal and latitudinal variability were not included. This model is extended now and we have calculated altitude profiles of the ion production rate of O_3^+ at fixed latitudes for different

This article is protected by copyright. All rights reserved.

Author Manuscript

seasons in MY28 and MY29. These calculations are made at low latitudes (2^{o}N, 2^{o}S, 25^{o}N and 25^{o}S), mid latitudes (45^o and 45^{o}S) and high latitudes (70^{o}N and 70^{o}S) between Ls ~ 0^o to 360^o and altitude ~ 0 to 60 km. The 2^o and 2 km resolutions are taken for Ls and altitude distributions respectively.

O' Brien et al. [1996] calculated the flux of un-attenuated GCR from 10^3 to 10^{-5} particles m^{-2} s^{-1} GeV^{-1} ster^{-1} at energy interval of 1 to 1000 GeV. We have assumed that this flux is precipitating into the lower atmosphere of Mars. We do not know what fraction of GCR impact at the top of the daytime atmosphere of Mars. In this model we have taken density profiles of O_3 from MCD for observing conditions of SPICAM. It should be noted that the un-attenuated GCR flux does not depend on season and latitude; therefore we have used the same flux in our calculation at different latitude and different solar longitudes. The modulation of cosmic rays is affected by the solar wind in the interplanetary medium. We have assumed that the solar wind interaction with cosmic rays is the same on Earth and Mars. Therefore, the same modulation of cosmic rays owing to the solar wind at Earth is used for Mars [*Molina-Cuberos* et al., 2002]. GCR is ionizing all atmospheric gases. Since the goal of this paper is to study the global cycle of O_3^+ therefore we have not included other gases of Mars in our model. Recently the high energy cosmic ray flux has been observed on the surface of Mars by the Radiation Assessment Detector (RAD) instrument onboard the Mars Science Laboratory (MSL) [*Ehresmann et al.*, 2014]. We have not used this flux in our model because the RAD

This article is protected by copyright. All rights reserved.

Author Manuscript

instrument observed mainly muon flux on the surface of Mars after attenuation of GCR through the atmosphere [*Haider* et al., 2015].

3.2 MCD Model

MCD is a database of Mars' meteorological fields derived from General Circulation Model (GCM). This model is validated using the available observed data [*Millour* et al., 2014]. The GCM has been developed in the Laboratoire de Meteorologic Dynamique du CNRS (Paris, France) under the collaboration of Open University (UK), Oxford University (UK), Institute de Astrofisica de Andalucia (Spain), and Centre National d' Etudes Spatiales (CNES). MCD is freely available online for the use of atmospheric and environmental research of Mars (website: http://www-mars.lmd.jussieu.fr). This model is developed for different scenarios of dust and solar conditions which are highly variable during short and long time scales. The UV radiation emitted from the sun is varying due to solar flares, 27 day solar rotation and the 11 year solar cycle. The atmosphere of Mars is also changing in the presence of low, medium and high dust storm periods. In the MCD model, the climatology scenario, cold scenario, warm scenario and dust scenario of the Mars atmosphere are provided for the modelling of the Martian ionosphere. In climatology scenario the solar minimum, medium and maximum conditions are provided for the study of Mars' atmosphere. The low dust is considered in the cold scenario corresponding to an extremely clear atmosphere. For a given seasonal date (Ls) and location, the dust opacity is set to be the minimum observed

This article is protected by copyright. All rights reserved.

Author Manuscript

over MY24-MY31. The warm scenario shows dusty atmosphere conditions but for a non-global dust storm period. The dust opacity at a given location and season is set to be the maximum observed over the MY 24- MY 31 except during the MY 25 and MY 28 intervals when global dust storms occurred. The effects of global dust storms are included in the dust scenario (The dust scenario represents the Mars' atmosphere in presence of global dust storms). The dust opacity is set to $\tau = 5$ during the dust storm period at a given location and season. Moreover the dust optical properties are for this case set to represent 'darker dust' than nominal [*Wolff* et al., 2009].

The MCD is based upon outputs from the LMD-MGCM model. The MGCM does include photochemistry, therefore the empirical MCD model also includes the species from the MGCM outputs. The MCD included photochemistry**,** dynamics and other metrological fields of the Martian atmosphere. These models calculate altitude profiles of air density, mixing ratios of CO_2, O_2, O, CO, O_3 , H, H_2, N_2, Ar and H_2O, neutral temperature, pressure and winds at different season, latitude and longitude in the dayside and nightside atmosphere above the surface of Mars for different scenarios (as given above).

We have taken altitude profiles (0 to 60 km) of ozone from the MCD model at low latitudes (2^oN, 2^oS, 25^oN and 25^oS), mid latitudes (45^oN and 45^oS) and high latitudes (70^oN and 70^oS) between Ls ~ 0^o and 360^o for dust storm and cold scenarios that occurred in MY 28 and MY 29 respectively. During MY 28 the density of ozone is larger

This article is protected by copyright. All rights reserved.

Author Manuscript

by a factor of ~3 than that estimated for MY 29 [*Millour* et al., 2014]. These densities are averaged over longitude. Later the zonally averaged profiles of ozone were integrated over altitude and compared with global cycle of column ozone density observed by SPICAM. This experiment also measured the vertical profiles of ozone in the night time atmosphere of Mars between altitude ~ 20 km and ~70 km from the stellar occultation method [*Lebonnois* et al., 2006; *Montmessin and Lefevre,* 2013]. No ozone was detected from this method down to ~ 20-30 km altitude. Ozone was also detected in the Martian atmosphere by Mariner 7 and 9 using Ultraviolet Spectrometers [*Barth and Hord*, 1971; *Barth* et al., 1973]. The altitude profiles of ozone are not measured in the daytime atmosphere of Mars. MCD has provided a complete set of global data of O_3 abundance during the daytime and night time atmosphere of Mars at all altitudes, latitudes and longitudes for different atmospheric conditions. Our objective is to study seasonal and altitude variability of the production rates of O_3^+ during the daytime above the surface of Mars in the presence and absence of dust storm in MY28 and MY29 respectively. In this model calculation daytime altitude profiles of ozone between 0 km and 60 km at low latitudes (2^oN, 2^oS, 25^oN and 25^oS), mid latitudes (45^oN and 45^oS) and high latitudes (70^oN and 70^oS) for Ls ~ 0 to 360^o are required. Therefore, we have not used night time density profiles of ozone observed by SPICAM in our model. The MCD model is providing all required inputs and can serve the objectives of this paper.

4. Results and Discussion

This article is protected by copyright. All rights reserved.

Author Manuscript

There have been observed several dust storms on Mars. Mariner 9 and Viking have detected two major dust storms in MY 10 and MY 13 respectively [*Martin*, 1984, 1995]. The infrared optical depths were increased to ~ 1.5 to 2.6 during these dust storms period. After two decades, the continuous remote sensing observations of infrared dust optical depths were carried out during MY 24 to MY 32 from MGS and Mars Odyssey spacecrafts [*Montabone* et al., 2015]. During these periods two major dust storms were observed in MY 25 and MY 28 with opacities 1.7 and 1.2 at Ls~ 210° and 280° respectively [*Montabone* et al., 2015; *Sheel and Haider*, 2016]. Recently a new global dust storm has been detected by the Opportunity Mars Exploration Rover (MER) and the Mars Reconnaissance Orbiter (MRO) in June, 2018 (MY34) (https://mars.nasa.gov/resources/21917/atmospheric-opacity-from-opportunitys-point-of-view). The previous dust storms in MY 10, MY 13, MY 25 and MY 28 were slower to build in comparison to the new dust storm of MY 34. The new dust storm observed maximum UV dust opacity $\tau = 10.8$ on June 10, 2018 at about Ls~ 190° and spread quickly all over the globe (https://www.nasa.gov/news/news.php). Our model result is dedicated to the previous dust storm ($\tau = 1.2$) that occurred in MY 28 at the southern tropical region (25°-35°S).

Figure 1 represents seasonal variability of zonal mean UV dust opacity measured by SPICAM in MY 28 and MY 29 [*Holmes* et al., 2018] at the southern tropical region (25°-35°S). These observations have been carried out from the nadir direction. The

This article is protected by copyright. All rights reserved.

Author Manuscript

optical depths are averaged over longitude. It is found that the dust optical depth increased by a factor of ~ 3 on the surface of Mars during southern summer at Ls ~ 280^o in MY 28. The minimum visible opacity of dust is observed ~ 0.2 μm in the cleaner southern winter season. The regional dust storms occurred in different seasons of Mars at optical depth τ = 0.5 to 0.75 between Ls ~ 0^o-50^o, 200^o and Ls~ 275^o-350^o. In this dust storm a large amount of dust lifted up into the atmosphere and formed two distinct layers at altitude range ~ 20-30 km and ~ 45-65 km [*Haider* et al., 2015]. These dust layers have been observed by CRISM and Mars Climate Sounder (MCS) onboard Mars Reconnaissance Orbiter [*Guzewich* et al., 2014; *Heavens* et al., 2014] (It should be noted that the dust optical depths obtained from SPICAM are generally larger than the results obtained from MER, MCS and CRISM [*Willame* et al., 2017]).

The total amount of O_3 in the atmosphere of Mars undergoes seasonal variation due to formation of the polar caps. Figures 2 (a-h) and 3 (a-h) represent the seasonal variability of zonally averaged column ozone observed by SPICAM in MY 28 and MY 29 respectively at low latitudes (2^{o}N, 2^{o}S, 25^{o}N and 25^{o}S), mid latitudes (45^{o}N and 45^{o}S) and high latitudes (70^{o}N and 70^{o}S). These observations are compared with the zonally averaged column ozone obtained from MCD in MY 28 and MY 29. The comparison of year-to year seasonal variability in column ozone shows strong similarity in MY 28 and MY 29 except at Ls ~ 280^o during the dust storm period which occurred in MY 28 at southern latitudes ~ 25^o-35^{o}S. The seasonal change in column ozone is low at low

This article is protected by copyright. All rights reserved.

latitudes, but at high latitudes it is chaotic and indicates that atmospheric ozone is highly perturbed.

At low latitudes (2^oN, 2^oS 25^oN and 25^oS) the observations do not match so well with the MCD model underestimating column ozone by ~20%. The disagreement between observation and model at low latitudes may be associated due to several reasons as given below: (1) The excessive transport of water vapor from Tharsis and Arabia Terrain can reduce column ozone in the model [*Steele* et al., 2014], (2) Modeling biases in water vapor can also explain the underestimation of total ozone at low latitude region [*Holmes* et al., 2018], (3) The SPICAM measurements have large error of the order of 1-5 x 10^{15} molecules cm^{-2} [*Lebonnois* et al., 2006]. The estimated column densities of ozone are varying within this error bar at low latitude region and (4) Ozone can also be affected by topography of Mars through the effect of gravity waves. An increase in O_3 column over Hellas basin in SPICAM measurements is attributed to a topographical induced transport of the polar air [*Clancy et al.*, 2016]. In Figures 2a-e and 2b-f we have plotted SPICAM and MCD profiles of ozone column density for their comparison in MY28 between northern and southern hemispheres at low latitudes 2^o N-S and 25^o N-S respectively. Similarly in Figures 3a-e and 3b-f we have also plotted SPICAM and MCD profiles of ozone column density for their comparison in MY29 between northern and southern hemispheres at low latitudes 2^o N-S and 25^o N-S respectively. In these figures two broad peaks (marked by arrow) are measured in the column ozone cycle with values

Author Manuscript

This article is protected by copyright. All rights reserved.

Author Manuscript

~ 5 x 10^{15} cm^{-2} and ~ 1 x 10^{16} cm^{-2} at Ls ~ 50^o and Ls ~ 250^o respectively. These peak values are larger by a factor of 5-10 than that produced by MCD model. In Figure 2f MCD model represents a 3^{rd} peak in the column ozone cycle with a value ~ 2 x 10^{15} cm^{-2} between Ls 150^o and 175^o. This peak may be produced due to the effect of regional dust storm on the ozone column density. The global dust storm of MY28 has been suggested to have several regional dust storms before the major dust storm [*Sheel and Haider*, 2016]. These major and regional dust storms have produced ~ 50% and ~ 30% reductions in the measured total water vapor content at Ls ~ 280^o and 175^o respectively [*Trokhimovskiy et al.*, 2014]. There is an anti-correlation between the abundances of ozone and water vapor. Therefore, the calculated column density of O_3 may increase in Figure 2f due to the effect of regional dust storm between Ls=150^o and 175^o. It should be noted that the SPICAM data is not available between Ls 100^o and 200^o at latitude 25^oS, therefore 3^{rd} peak is not observed in Figure 2f.

At mid-to high latitudes (45^oN, 45^oS, 70^oN and 70^oS) the ozone column densities are maximum in northern winter and minimum in southern summer**.** In both hemispheres the column densities of ozone are lower at mid latitudes by a factor of 2-5 than the column densities of ozone at high latitudes. In northern hemisphere the ozone is not measured between Ls ~ 250^o and 350^o at mid-to high latitudes. At these latitudes the seasonal profiles of column ozone obtained from MCD are generally in good agreement with the SPICAM observations except in Figures 2h and 3h at latitude 70^oS. In these

This article is protected by copyright. All rights reserved.

Author Manuscript

figures we notice that the column ozone observed by SPICAM in MY28 and MY29 are higher than the MCD derived column ozone by a factor of ~ 5 to 8 between Ls 230°-300° and 300°-330° respectively. This enhancement in the column ozone was observed due to high dust opacity ~ 1.5 [*Willame et al.*, 2017].

Figure 4 represents zonal mean column ozone obtained from MCD as a function of solar longitude between Ls ~ 250° and 350° at latitude 25°S in MY 28 and MY 29. In presence of the dust storm a major dust layer is formed above the surface of Mars [*Guzewich* et al., 2014; *Heavens* et al., 2014; *Haider et al.*, 2015]. During the thick layer of dust, the sunlight cannot penetrate deep into the atmosphere of Mars. This interrupts the dissociation of ozone below the dust layer, which is the main loss mechanism of ozone in dayside atmosphere. On the other hand production of O_3 is directly related to the production of the oxygen atom, which is produced more above the dust layer from the photolysis of CO_2. Therefore the integrated column O_3 will be enhanced during the dust storm period. In Figure 4 we have found that O_3 column density is enhanced by a factor of ~ 2.6 at Ls ~ 280° during the dust storm of MY28. Recently *Liu et al.* (2018) have observed neutral densities of CO_2, Ar, N_2, CO, and O at high altitudes from 170 to 220 km in response to dust increases in the lower atmosphere, observed by the in situ Neutral Gas Ion Mass Spectrometer (NGIMS) onboard the Mars Atmosphere and Volatile Evolution (MAVEN) satellite. These observations reveal that the densities of all atmospheric gases increase up to ~ 200% in the presence of dust storm. The

This article is protected by copyright. All rights reserved.

Author Manuscript

thermospheric density increases caused by dust have also been reported earlier using the observations made by Accelerometer experiment (ACC) onboard MGS [*Keating et al*., 1998; *Bougher et al*., 1999, 2017].

Figure 5 (a-h) represents the annual variability of the zonal mean production rates of O_3^+ on the surface of Mars in MY 28 and MY 29 at four low latitudes (2^{o}S, 2^{o}N, 25^{o}S and 25^{o}N), two mid-latitudes (45^{o}S and 45^{o}N) and two high latitudes (70^{o}S and 70^{o}N). These production rates are estimated from the seasonally dependent energy loss model by using MCD model derived ozone column densities. At mid-to-high latitudes (Figures 5c, 5d, 5g and 5h) maximum and minimum ion production rates are calculated during northern winter and southern summer respectively while minimum and maximum ion production rates were estimated during northern summer and southern winter respectively. At low northern and southern latitudes (Figures 5a, 5b, 5e and 5f) two crests and one trough are produced in each annual cycle of the production rates of O_3^+ at Ls ~ 50^o-100^o, Ls ~ 200^o-300^o and Ls ~ 150^o respectively. These crests and trough are produced at low latitudes due to the Hadley asymmetric circulation [cf. *Millour* et al., 2014]. The annual cycle of the production rates of O_3^+ are nearly same in MY28 and MY29 except for the dust storm period as shown in Figure 5f. This is due to the fact that MCD derived column density of O_3 is enhanced between Ls = 250^o and Ls = 350^o at latitude 25^o S in MY28 (see Figure 4). In Figure 5f we have used this column density of O_3 for the calculation of the ion production rate of O_3^+.

This article is protected by copyright. All rights reserved.

Author Manuscript

Since the altitude profiles of the production rates of O_3^+ are nearly same in MY 28 and MY 29 at the same latitudes and same seasons we have plotted these profiles in Figures 6 (a, b), 7 (a, b), 8 (a, b) and 9 (a, b) at latitudes 2^{o}N-S, 25^{o}N-S, 45^{o}N-S and 70^{o}N-S respectively for MY 28 only. In Figures 6a, 7a, 8a and 9a we represent the altitude profiles of the production rates of O_3^+ at northern latitudes 2^{o}N, 25^{o}N, 45^{o}N and 70^{o}N respectively for Ls ~ 7.5^o, 47.5^o, 87.5^o, 127.5^o, 167.5^o, 207.5^o, 247.5^o, 287.5^o and 327.5^o. Figures 6b, 7b, 8b and 9b represent the same profiles of the production rates of O_3^+ but at southern latitudes 2^{o}S, 25^{o}S, 45^{o}S and 70^{o}S respectively. Table 1 represents the peak altitudes and peak production rates of O_3^+ in MY28 at Ls ~ 7.5^o, 47.5^o, 87.5^o and 127.5^o for latitudes 2^{o}N-S, 25^{o}N-S and 45^{o}N-S. At these latitudes the peak production rates of O_3^+ increased up to Ls ~ 47.5^o with maximum value ~ 2.5 x 10^{-8} cm^{-3} s^{-1}. Later it decreased up to Ls ~ 127.5^o and then disappeared at Ls ~ 167.5^o, 207.5^o, 247.5^o, 287.5^o and 327.5^o. The clear peaks are found in these production rates between altitudes 26 km and 45 km. The production layer of O_3^+ is higher in altitude at low latitudes and lower in altitude at mid latitudes, especially in southern region. The ionization peaks do not occur in the troposphere of Mars at polar latitudes ~70^{o}N and 70^{o}S.

At latitudes 45^{o}N, 45^{o}S, 70^{o}N and 70^{o}S the surface production rates of O_3^+ are increasing by two orders of magnitude in northern winter due to condensation of CO_2 frost. At these latitudes the surface production rates of O_3^+ are decreasing by two orders of magnitude in southern summer due to sublimation of CO_2 frost. During summer, polar

This article is protected by copyright. All rights reserved.

Author Manuscript

caps are releasing water vapor which destroys the ozone [*Lefevre* et al., 2008]. This process does not occur in northern polar winter which is too cool and protected from the formation of odd hydrogen species, which significantly contributes in the destruction of ozone. The ozone concentration peak at low-to mid latitudes can be obtained in both hemispheres between altitudes 25 km and 45 km at Ls ~7.5^o, 47.5^o, 87.5^o and 127.5^o from the photolysis of O_2 which combines with O and forms the O_3 layer [*Lefevre* et al., 2004]. This layer is fully destroyed by photodissociation. These peak heights are reduced by about 10-20 km at southern mid latitudes in comparison to northern mid-latitudes. These peaks are not found in the production rates of O_3^+ at high latitudes in all seasons of both hemispheres.

The SPICAM has observed two distinct ozone layers in the nighttime atmosphere of Mars at low-to mid latitudes [*Lebonnois* et al., 2006]. The first layer occurred near the surface. The second layer was observed between altitudes 25 km and 60 km. Later *Montmessin and Lefevre* [2013] observed a broad peak in the vertical profiles of ozone at altitudes between 40 km and 60 km in southern polar night, which was overlooked by *Lebonnois* et al. [2006]. The nighttime ozone layer is produced due to horizontal transport of oxygen atoms from the dayside into the nightside atmosphere across the terminator [*Montmessin and Lefevre,* 2013]. We have not detected any peak in the daytime vertical profiles of the production rates of O_3^+ near the surface. Our study suggests that the mechanisms of ozone formation in the dayside and nightside atmosphere

This article is protected by copyright. All rights reserved.

of Mars are different at low, mid and high latitudes. The dust increases the ion production rate by a factor of 3-4 on the surface in MY 28 (Figure 5f). The effects of dust on the production rate is nearly absent beyond ~ 10 km altitude (Figure 7b). The peak production rate of O_3^+ is directly correlated with the abundance of ozone. GCR does not produce ionization peaks but it is attenuated throughout the atmosphere in the production rates of O_3^+.

5. Summary and Conclusions

We have developed a seasonally dependent energy loss model to study the annual variability of the ion production rates of O_3^+ due to impact of GCR in the daytime ionosphere of Mars at low, mid and high latitudes. These calculations are carried out in MY 28 and MY 29 between Ls ~ 0^o-to 360^o and altitudes 0-to 60 km at latitudes 2^oN-S, 25^oN-S, 45^oN-S and 70^oN-S. We also represent seasonal variability of zonal mean ozone column density obtained from the MCD model at different latitudes in MY 28 and MY 29. These results are compared with the daytime observations of the column ozone made by SPICAM onboard MEX. It is found that the ozone column density maximizes in northern winter and minimizes in southern summer at mid-to high latitudes. The ion production rates of O_3^+ represent a broad peak between 30-to 40 km in both hemispheres at low-to mid latitudes. The peak production rates are increasing up to Ls=47.5^o and then decreasing until they disappear after Ls = 127.5^o. There are no ionization peaks in these production rates at polar latitudes.

Author Manuscript

This article is protected by copyright. All rights reserved.

Author Manuscript

A major dust storm occurred in MY 28 at Ls~ 280° in southern tropical latitudes (25°-35°S). During the storm period the dust opacity, ozone column density and production rates of O_3^+ were increased on the surface of Mars by a factor of 3-4. The altitude profiles of ozone are not measured in the daytime atmosphere of Mars. These profiles are measured in the nighttime only by the stellar occultation method [*Montmessin and Lefevre*, 2013]. Using a detailed computational study of seasonal dependent energy loss model we found that the production rates of O_3^+ are strongly changing with season and latitude due to different chemical processes of ozone formation in the daytime atmosphere of Mars. The mechanisms of ozone layer formation are substantively different in different seasons at low, mid and high latitudes. This theoretical prediction awaits experimental validation and in the absence of ozone measurements in the dayside atmosphere of Mars, our results can serve as a benchmark that can guide the design of future payloads of ozone measurements on Mars.

Acknowledgments:

SPICAM instrument was designed and fabricated by three institutes: Service d' Aeronomie, France, BIRA, Belgium and IKI, Moscow. We wish to express our gratitude to all members of SPICAM team who participated in this project. SPICAM data has been provided us by F. Lefevre (franck.lefevre@aero.jussieu.fr) and is freely available at ftp://psa.esac.int/pub/mirror/MARS-EXPRESS/SPICAM/. We also thank to F. Lefevre and his team for their support. Authors also acknowledge MCD data team: E. Millour

This article is protected by copyright. All rights reserved.

(millour@lmd.jussieu.fr) and F. Forget (francois.forget@lmd.jussieu.fr) for providing freely accessible Mars Climate data at http://www-mars.lmd.jussiey.fr. S.A. Haider and Y. Siddhi acknowledge the support of J.C. Bose grant for supporting to carry out this work.

Author Manuscript

Table 1- Peak altitudes and peak production rate of O_3^+ in MY 28

This article is protected by copyright. All rights reserved.

Author Manuscript

Latitude	**Ls**	**Peak altitude (km)**	**Peak production rate ($cm^{-3}s^{-1}$)**
2^oN	7.5^o	35	4.0×10^{-9}
	47.5^o	40	2.5×10^{-8}
	87.5^o	38	1.3×10^{-8}
	127.5^o	36	2.0×10^{-9}
2^oS	7.5^o	36	4.1×10^{-9}
	47.5^o	39	2.5×10^{-8}
	87.5^o	36	1.2×10^{-8}
	127.5^o	37	2.0×10^{-9}
25^oN	7.5^o	42	4.0×10^{-9}
	47.5^o	39	2.0×10^{-8}
	87.5^o	41	1.5×10^{-8}
	127.5^o	45	2.0×10^{-9}
25^oS	7.5^o	38	4.1×10^{-9}
	47.5^o	36	1.6×10^{-8}
	87.5^o	39	1.2×10^{-8}
	127.5^o	40	1.6×10^{-9}
45^oN	7.5^o	40	3.5×10^{-9}
	47.5^o	42	1.5×10^{-8}
	87.5^o	43	1.0×10^{-8}
	127.5^o	41	1.8×10^{-9}
45^oS	7.5^o	26	1.0×10^{-8}
	47.5^o	30	1.5×10^{-8}
	87.5^o	28	4.0×10^{-9}
	127.5^o	32	1.2×10^{-9}

This article is protected by copyright. All rights reserved.

Author Manuscript

References

Barth, C. A., and C.W. Hord (1971), Mariner ultraviolet spectrometer: Topography and polar cap. *Science, 173 (3993),* 197-201.

Barth, C. A., C.W. Hord, A. I. Stewart, A. L. Lane, M. L. Dick, and G. P. Anderson (1973), Mariner 9 ultraviolet spectrometer experiment: Seasonal variation of ozone on Mars. *Science, 179 (4075)*, 795-796.

Bertaux, J. L., O. Korablev, S. Perrier, E. Quemerais, F. Montmessin, F. Leblanc, S. Lebonnois, P. Rannou, F. Lefèvre, F. Forget, and A. Fedorova (2006), SPICAM onboard Mars Express: Observing modes, and overview of typical results. *J. Geophys. Res., 111 (E10)*, 925-940.

Bougher, S. W., S. Engel, R. G. Roble, and B. Foster (1999), Comparative terrestrial planet thermospheres: 2. Solar cycle variation of global structure and winds at equinox,J. Geophys. Res.,104 (E7), 16,591–16,611, doi:10.1029/1998JE001019.

Bougher, S.W., K.J. Roeten, K. Olsen, P.R. Mahaffy, M. Benna, M. Elrod, S.K. Jain, N.M. Schneider, J. Deighan, E. Thiemann, and F.G. Eparvier (2017), The structure and variability of Mars dayside thermosphere from MAVEN NGIMS and IUVS measurements: Seasonal and solar activity trends in scale heights and temperatures. *J. Geophys. Res., 122 (1*), 1296-1313.

This article is protected by copyright. All rights reserved.

Author Manuscript

Clancy, R. T., M.J. Wolff, F. Lefèvre, B.A. Cantor, M.C. Malin, and M.D. Smith (2016), Daily global mapping of Mars ozone column abundances with MARCI UV band imaging. *Icarus*, *266*, 112-133.

Ehresmann, B., et al. (2014), Charged particle spectra obtained with the Mars Science Laboratory Radiation Assessment Detector (MSL/RAD) on the surface of Mars. *J. Geophys. Res.*, *119 (3)*, 468-479.

Guzewich, S.D., M.D. Smith, and M.J. Wolff (2014), The vertical distribution of Martian aerosol particle size. *J. Geophys. Res.*, *119 (12)*, 2694-2708.

Haider, S. A., V. Sheel, M. D. Smith, W. C. Maguire, G. J. Molina-Cuberos (2010), Effect of dust storm on the D region of the Martian ionosphere: Atmospheric electricity, J. Geophys. Res., 115(A12), Doi:10.1029/2010JA016125.

Haider, S. A., et al. (2009), D, E, and F layers in the daytime at high-latitude terminator ionosphere of Mars: Comparison with Earth's ionosphere using COSMIC data. *J. Geophys. Res.*, *114*, A03311, doi:10.1029/2008JA013709.

Haider, S. A., V. Sheel, V. Singh, W.C. Maguire, and G.J. Molina-Cuberos (2008), Model calculation of production rates, ion and electron densities in the evening troposphere of Mars at latitudes 67°N and 62°S: Seasonal variability. *J. Geophys. Res. 113*, A08320, doi:1.1029/2007JA012980.

Haider, S. A., V. Singh, V.R. Choksi, W.C. Maguire, and M.I. Verigin (2007), Calculated densities of $H_3O^+(H_2O)_n$, $NO_2^-(H_2O)_n$, $CO_3^-(H_2O)_n$ and electron in the nighttime

This article is protected by copyright. All rights reserved.

Author Manuscript

ionosphere of Mars: Impact of solar wind electron and galactic cosmic rays. *J. Geophys. Res. 112 (A12)*, A12309, doi:10.1029/2007JA012530.

Haider, S. A., I. S. Batista, M. A. Abdu, P. Muralikrishna, S.Y. Shah, and T. Kuroda (2015). Dust storm and electron density in the equatorial D region ionosphere of Mars: Comparison with Earth's ionosphere from rocket measurements in Brazil. *J. Geophys. Res., 120*, 8968-8977, doi:10.1002/2015JA021630.

Heavens, N. G., M.S. Johnson, W.A. Abdou, D.M. Kass, A. Kleinböhl, D.J. McCleese, J.H. Shirley, and R.J. Wilson (2014), Seasonal and diurnal variability of detached dust layers in the tropical Martian atmosphere, *J. Geophys. Res. Planets*, *119*, 1748-1774.

Holmes, J.A., S.R. Lewis, M.R. Patel, and F. Lefèvre (2018), First ozone reanalysis on Mars using SPICAM data. In: From Mars Express to ExoMars, 27-28 Feb 2018, Madrid.

Keating, G.M., S.W. Bougher, R.W. Zurek, R.H. Tolson, G.J. Cancro, S.N. Noll, J.S. Parker, T.J. Schellenberg, R.W. Shane, B.L. Wilkerson, and J.R. Murphy (1998), The structure of the upper atmosphere of Mars: In situ accelerometer measurements from Mars Global Surveyor*, Science, 279 (5357),* 1672-1676.

Lebonnois, S., E. Quémerais, F. Montmessin, F. Lefèvre, S. Perrier, J.L. Bertaux, and F. Forget (2006), Vertical distribution of ozone on Mars as measured by SPICAM/Mars Express using stellar occultations. *J. Geophys. Res., 111(E9).*

This article is protected by copyright. All rights reserved.

Author Manuscript

Lefèvre, F., et al. (2008), Heterogeneous chemistry in the atmosphere of Mars. *Nature,* 454 (7207).

Lefevre, F., S. Lebonnois, F. Montmessin, and F. Forget (2004), Three-dimensional modeling of ozone on Mars, J. Geophys. Res., 109, E07004, doi:10.1029/2004JE002268.

Liu, G., S.L. England, R.J. Lillis, P. Withers, P. R. Mahaffy, D. E. Rowland, M. Elrod, M. Benna, D. M. Kass, D. Janches, and B. M. Jakosky (2018), Thermospheric expansion associated with dust increase in the lower atmosphere on Mars observed by MAVEN/NGIMS. *Geophys. Res. Lett.*, *45(7)*, 2901-2910.

Martin, L.J. (1984), Clearing the Martian air: The troubled history of dust storms, *Icarus, 57(3)*, 317-321.

Martin, T.Z. (1995), Mass of dust in the Martian atmosphere, *J. Geophys. Res., 100,* 7509–7512.

Michael, M., M. Barani, S. N. Tripathi (2007), Numerical predictions of aerosol charging and electrical conductivity of the lower atmosphere of Mars, *Geophys. Res. Lett.* 34, L04201, Doi:10.1029/2006GL028434.

Millour, E., et al. (2014), A new Mars climate database v5.1, paper 1301 presented at The Fifth International Workshop on Mars Atmosphere: Modeling and Observations, Oxford, U. K., Jan. 2014.

This article is protected by copyright. All rights reserved.

Author Manuscript

Molina-Cuberos, G.J., H. Lichtenegger, K. Schwingenschuh, J.J López Moreno, R. Rodrigo (2002), Ion neutral chemistry model of the lower ionosphere of Mars. *J. Geophys. Res., 107(E5).* DOI: 10.1029/2000JE001447

Molina-Cuberos, G.J. et al (2006), Schumann resonances as a tool to study the lower ionospheric structure of Mars, *Radio Sci.*, 41, Doi:10.1029/2004RS003187.

Montabone, L., et al. (2015), Eight-year climatology

Icarus, 251, 65–95.

Montmessin, F., and F. Lefèvre (2013), Transport-driven formation of a polar ozone layer on Mars, *Nature, 6(11),* 930.

Montmessin, F., O. Korablev, F. Lefèvre, J.L. Bertaux, A. Fedorova, A. Trokhimovskiy, J.Y. Chaufray, G. Lacombe, A. Reberac, L. Maltagliati, and Y. Willame (2017), SPICAM on Mars Express: a 10 year in-depth survey of the Martian atmosphere, *Icarus, 297*, 195-216.

O'Brien, K., W. Friedberg, H. H. Sauer, and D. F. Smart (1996), Atmospheric cosmic rays and solar energetic particles at aircraft altitudes, Environ. Int., 22, (suppl. 1), S9–S44.

Sheel, V., and S.A. Haider (2016), Long-term variability

during MY24–MY32 and their impact on subtropical lower ionosphere: Climatology, modeling, and observations, *J. Geophys. Res., 121(8),* 8038-8054.

This article is protected by copyright. All rights reserved.

Author Manuscript

Smith, M. D. (2009), THEMIS observations of Mars aerosol optical depth from 2002-2008, *Icarus*, *202*, 444-452, doi:10.1016/jicarus2009.03.027.

Smith, M.D., M.J. Wolff, R.T. Clancy, A. Kleinböhl, and S.L. Murchie (2013), Vertical distribution of dust and water ice aerosols from CRISM limb -geometry observations, *J. Geophys. Res., 118(2),* 321-334.

Steele, L.J., S. R. Lewis, M. R. Patel, F. Montmessin, F. Forget, and M.D. Smith (2014), The seasonal cycle of water vapour on Mars from assimilation of Thermal Emission Spectrometer data, *Icarus, 237,* 97-115.

Thomas P. and P. J. Gierasch (1985), Dust devil on Mars, Science, 230, 175-177.

Tolendo-Redondo et al (2017), Schumann resonances at Mars: Effects of the dy-night asymmetry and dust loaded ionosphere, *Geophys. Res., Lett.*, 44, 648-656, Doi:10.1002/2016GL071635

Trokhimovskiy, A., A. Fedrova, O. Korablev, F. Montmessin, J. L. Bertaux, A. Rodin, and M.D. Smith (2015), Mars' water vapor mapping by SPICAM IR spectrometer: Five Martian years of observations, *Icarus*, 251, 50-64, doi:10.1016/j.icarus.2014.10.007.

Whitten, R. C., I. G. Poppoff, and J .S. Sims (1971), The ionosphere of Mars below 80 km altitude-I. Quiescent conditions, *Planet. Space Sci, 19*, 243-250, doi: 10.1016/0032-0633 (71) 90203-0.

This article is protected by copyright. All rights reserved.

Willame, Y., A.C. Vandaele, C. Depiesse, F. Lefèvre, V. Letocart, D. Gillotay, and F. Montmessin (2017), Retrieving cloud, dust and ozone abundances in the Martian atmosphere using SPICAM/UV nadir spectra, *Planet. Space Sci., 142*, 9-25.

Wolff, M. J., M.D. Smith, R.T. Clancy, R. Arvidson, M. Kahre, F. Seelos, S. Murchie, and H. Savijärvi (2009), Wavelength dependence of dust aerosol single scattering albedo as observed by the Compact Reconnaissance Imaging Spectrometer, *J. Geophys. Res., 114 (E2).*

Author Manuscript

This article is protected by copyright. All rights reserved.

Author Manuscript

Figure captions

Figure 1. The annual seasonal variability of zonal mean UV dust optical depth observed by SPICAM in MY 28 and MY 29 at southern tropical region (25°-35°S).

Figure 2. The annual seasonal variability of zonally averaged column ozone with error bars as observed by SPICAM in MY 28 at 2°N (a), 25°N (b), 45°N (c), 70°N (d), 2°S (e), 25°S (f), 45°S (g), and 70°S (h). These observations are compared with zonally averaged column ozone obtained from MCD model in MY 28. The arrow shows the two major peaks in ozone column cycle at Ls ~50° and ~250° in MY28 at latitudes 2°N, 2°S, 25°N and 25°S in Figures 2a, 2e, 2b and 2f respectively.

Figure 3. Same as in figure 2 but for My 29.

Figure 4. The zonal mean column ozone obtained from MCD model as a function of solar longitude (Ls) between Ls=250° and Ls=350° at latitude 25°S in MY 28 and My 29.

Figure 5. The annual variability of zonal mean production rates of O_3^+ on the surface of Mars in MY 28 and MY 29 at latitudes 2°N (a), 25°N (b), 45°N (c), 70°N (d), 2°S (e), 25°S (f), 45°S (g) and 70°S (h).

Figure 6. The altitude profiles of the production rates of O_3^+ in MY 28 at latitudes 2°N (a) and 2°S (b) for Ls = 7.5°, 47.5°, 87.5°, 127.5°, 167.5°, 207.5°, 247.5°, 287.5° and 327.5°.

This article is protected by copyright. All rights reserved.

Figure 7. Same as in figure 6 but for latitudes 25°N (a) and 25°S (b).

Figure 8. Same as in figure 6 but for latitudes 45°N (a) and 45°S (b).

Figure 9. Same as in figure 6 but for latitudes 70°N (a) and 70°S (b).

Author Manuscript

This article is protected by copyright. All rights reserved.

Author Manuscript

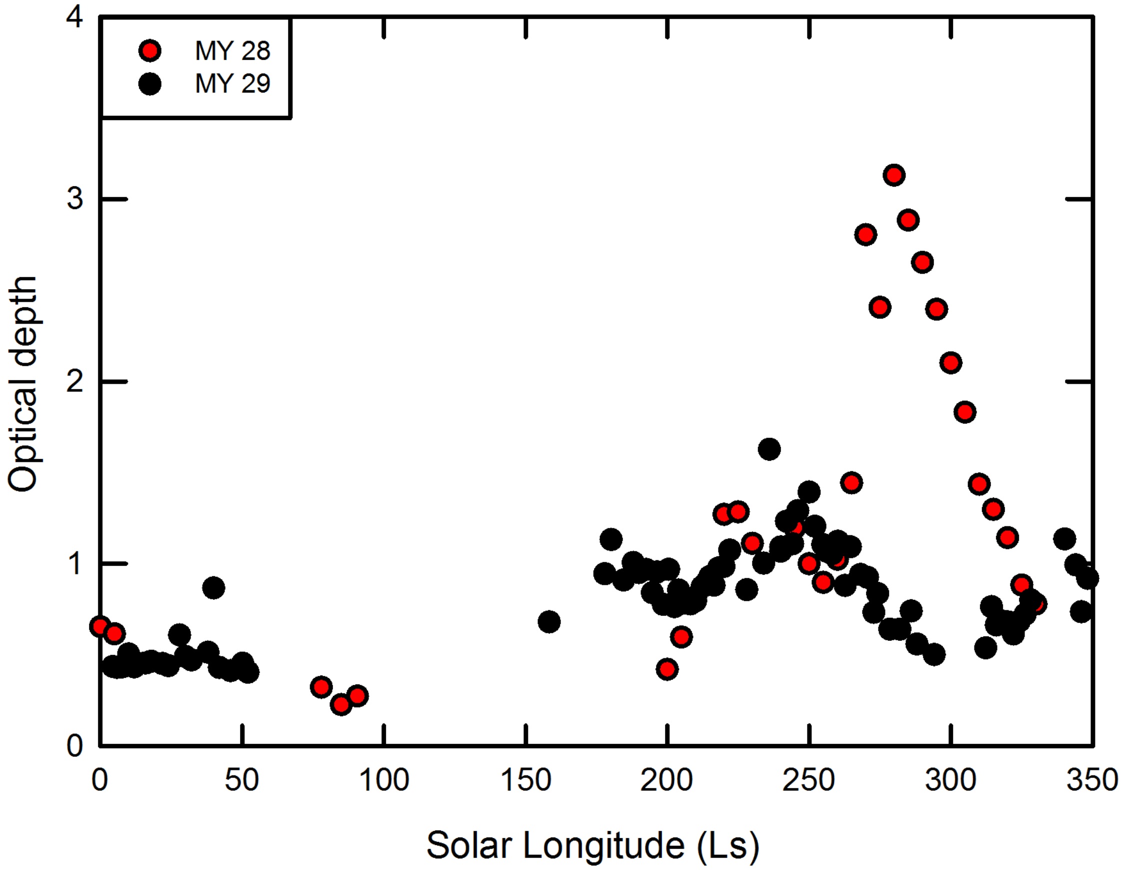

This article is protected by copyright. All rights reserved.

Author Manuscript

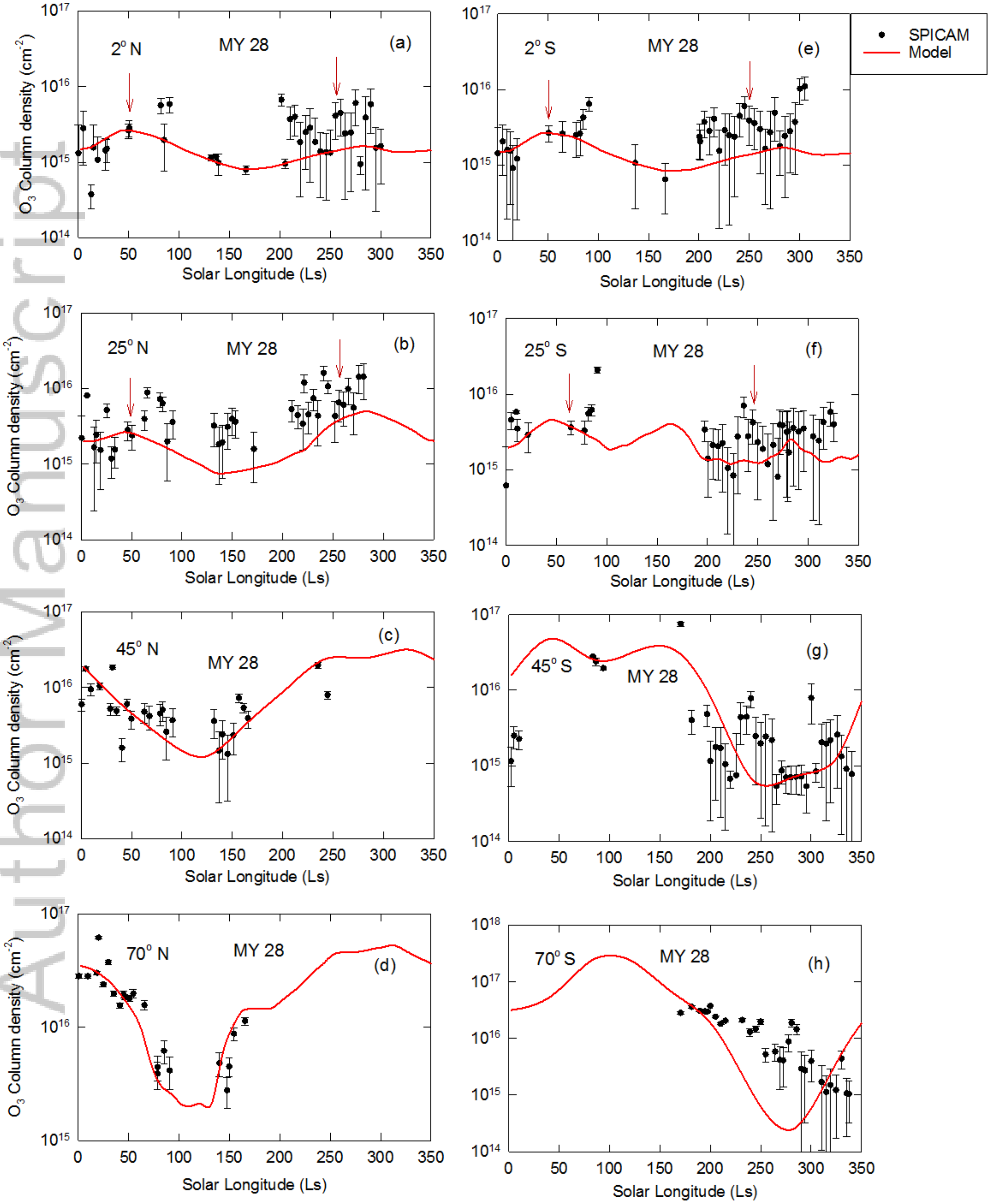

This article is protected by copyright. All rights reserved.

Author Manuscript

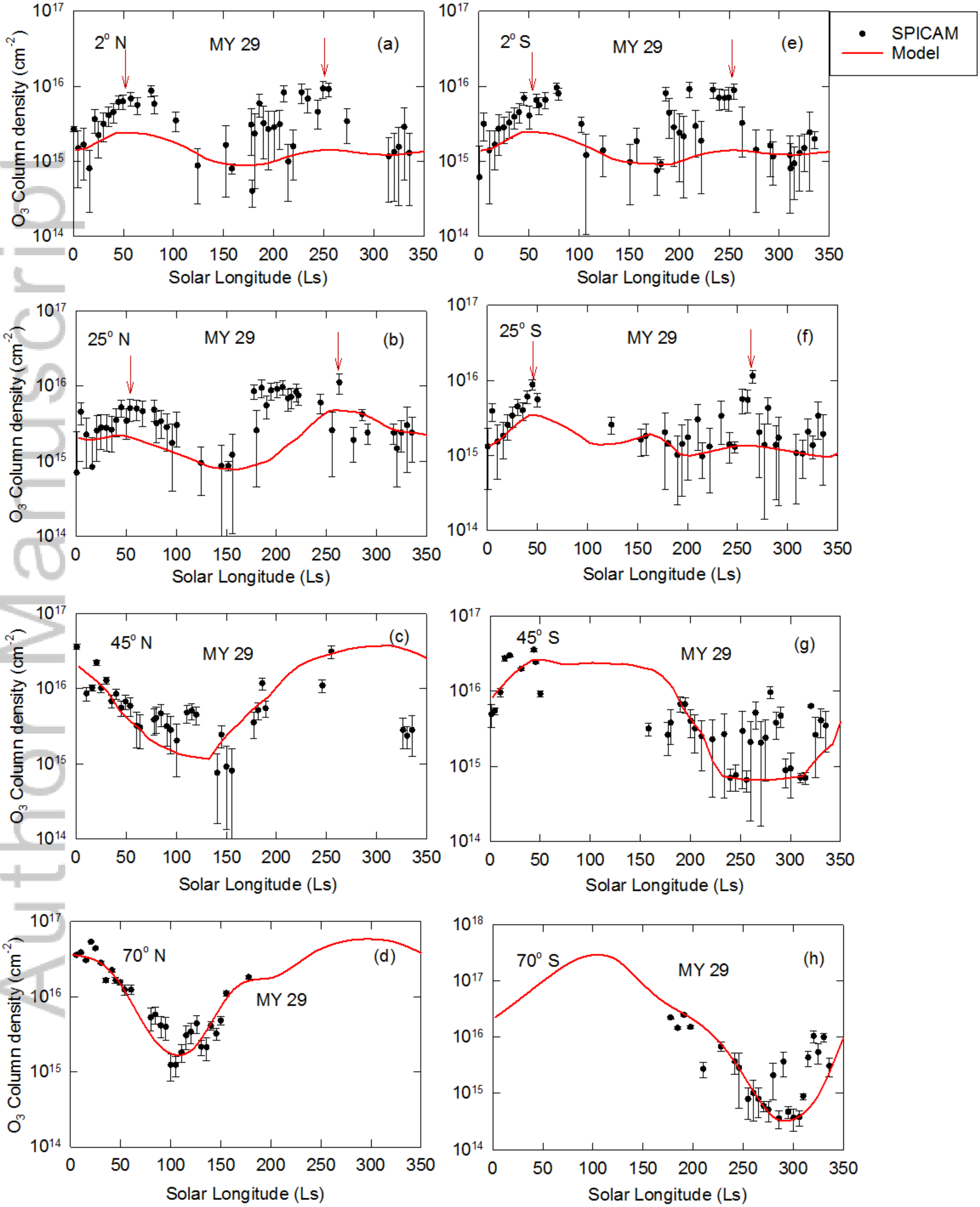

This article is protected by copyright. All rights reserved.

Author Manuscript

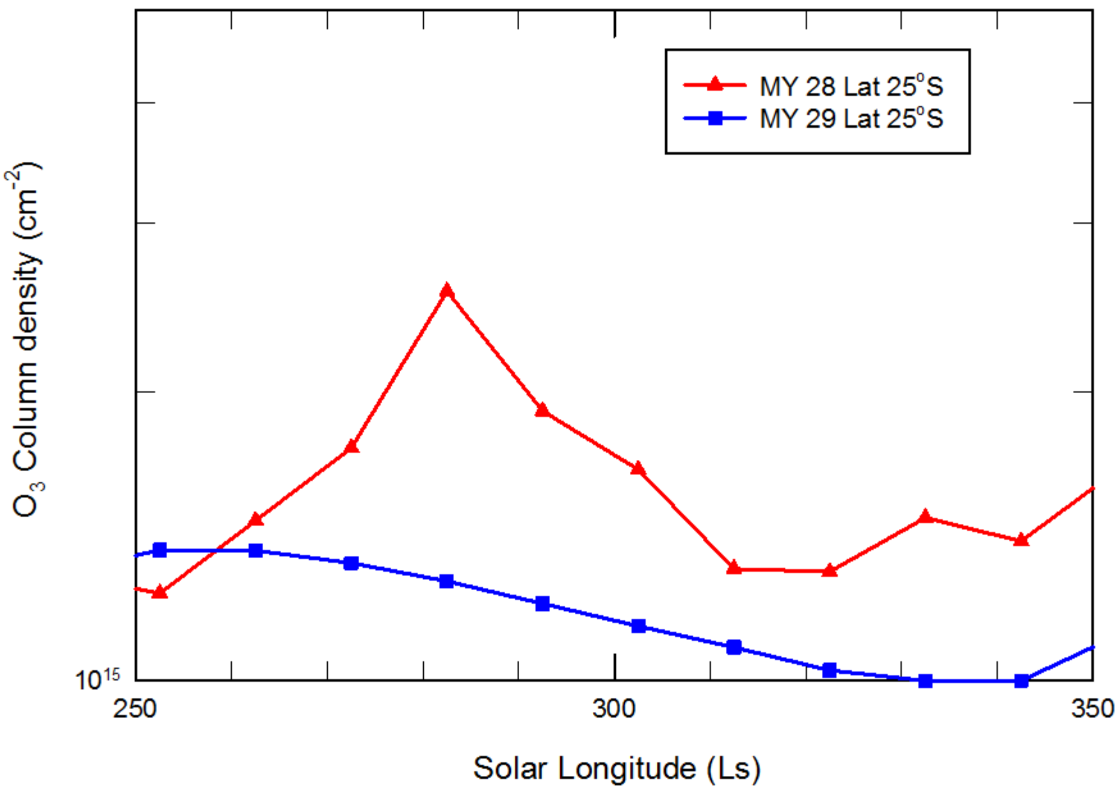

This article is protected by copyright. All rights reserved.

Author Manuscript

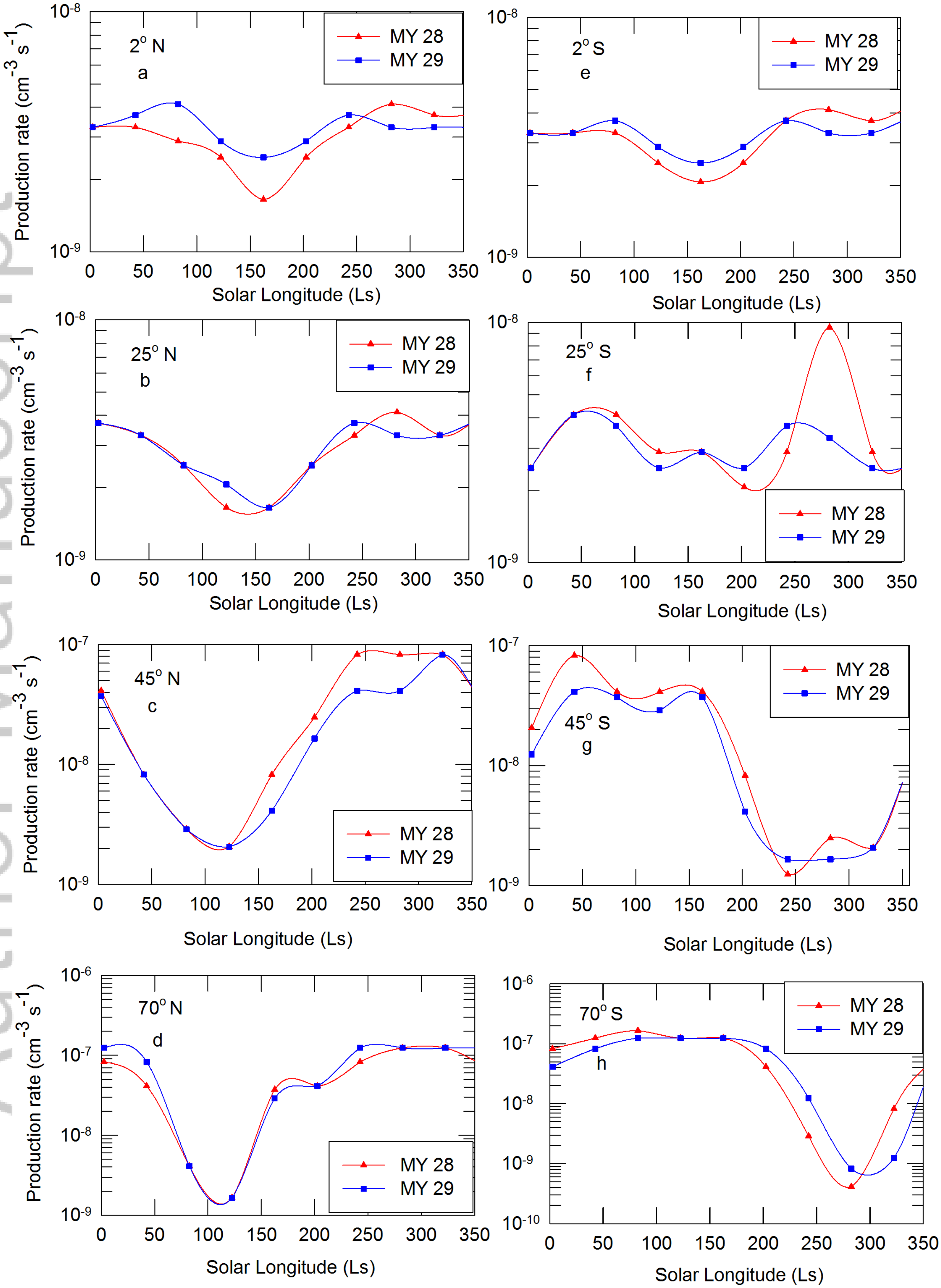

This article is protected by copyright. All rights reserved.

Author Manuscript

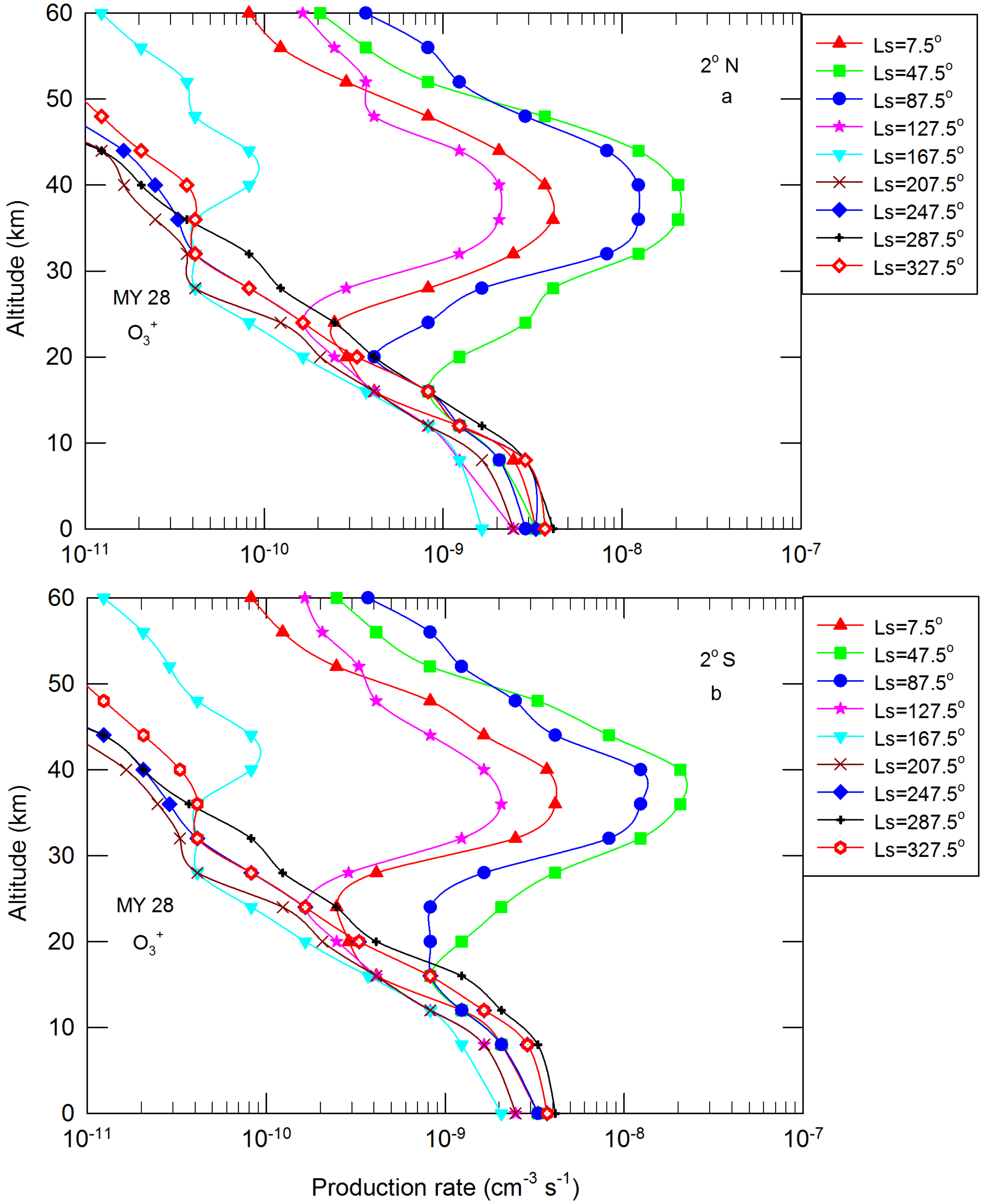

This article is protected by copyright. All rights reserved.

Author Manuscript

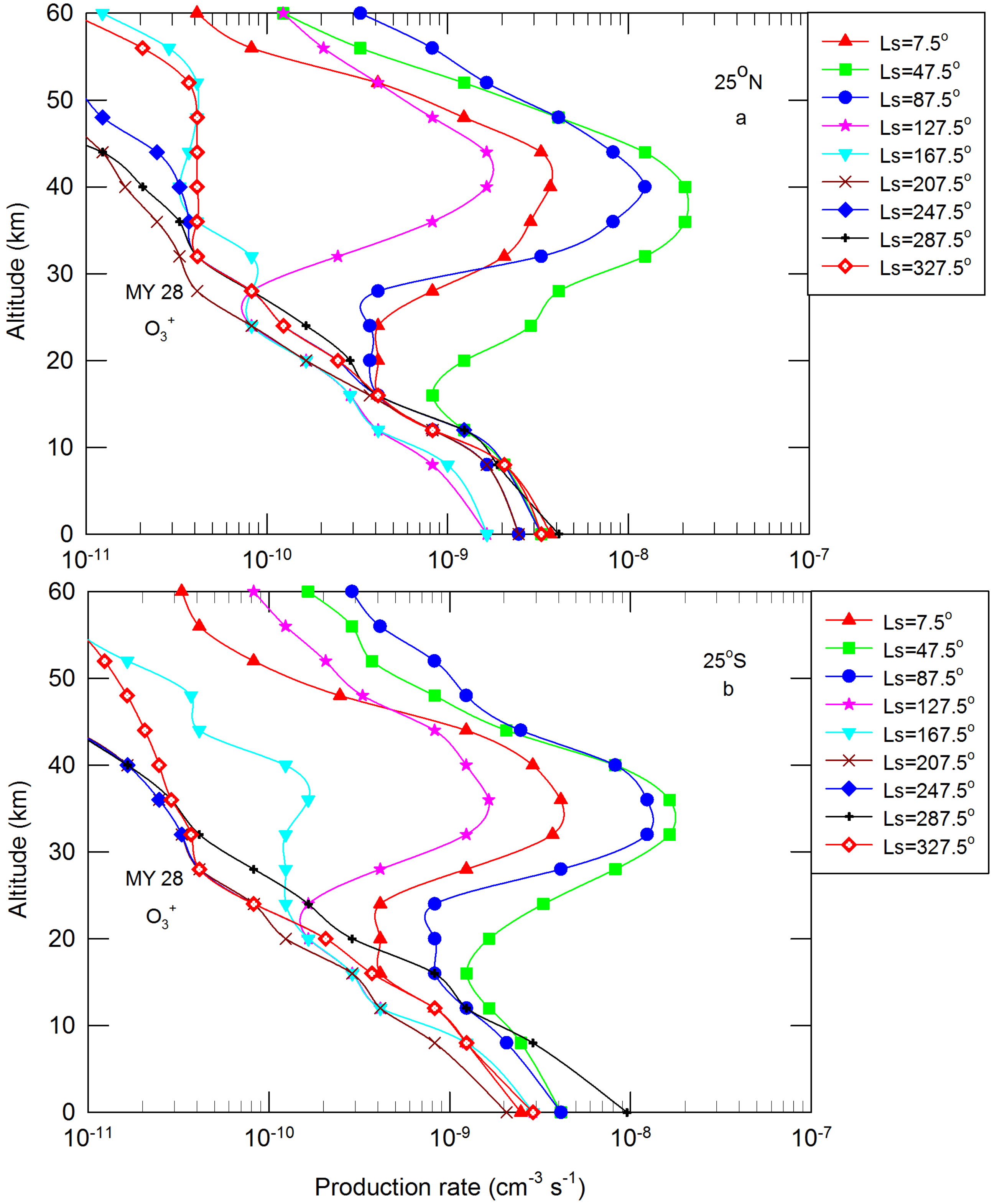

This article is protected by copyright. All rights reserved.

Author Manuscript

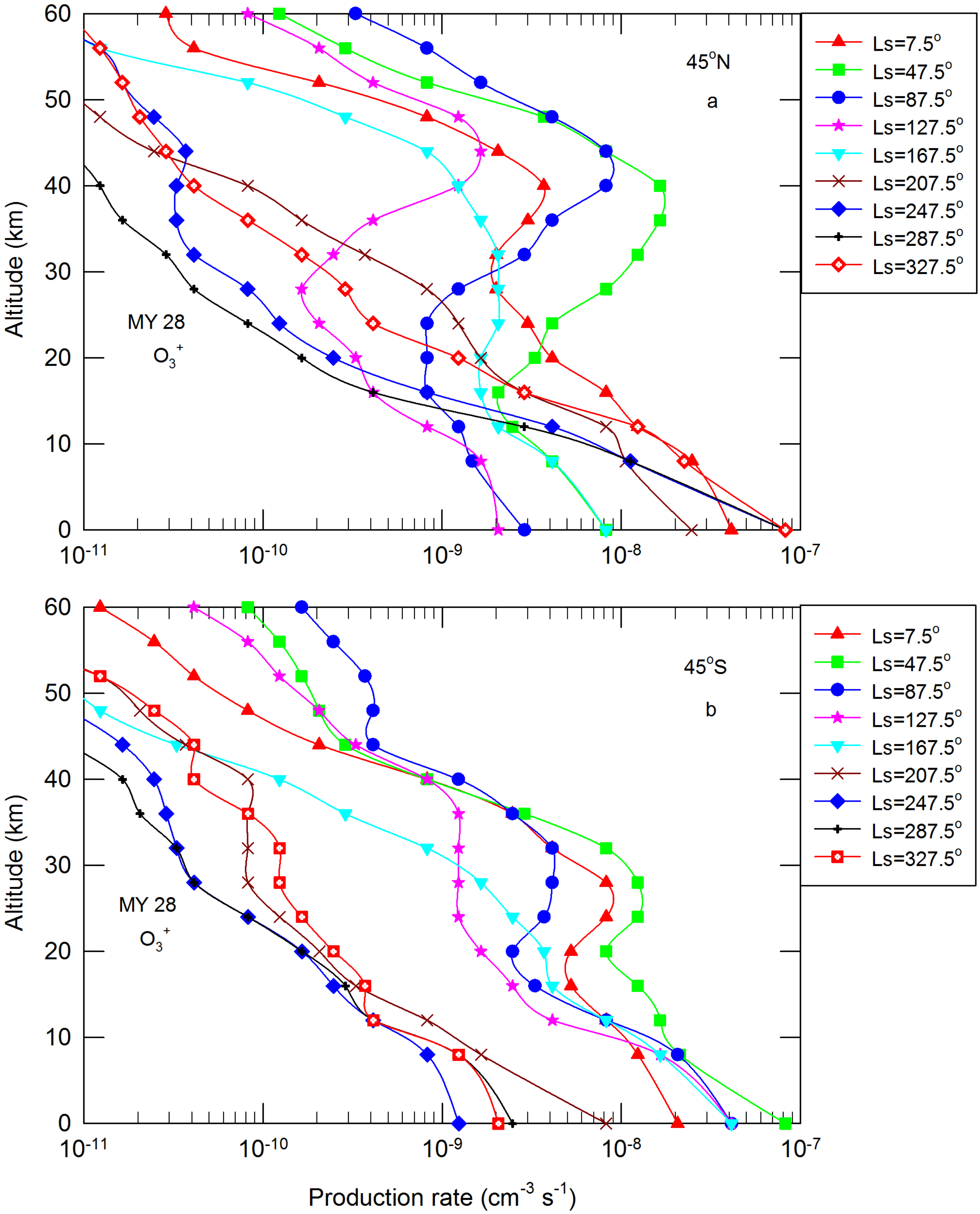

This article is protected by copyright. All rights reserved.

Author Manuscript

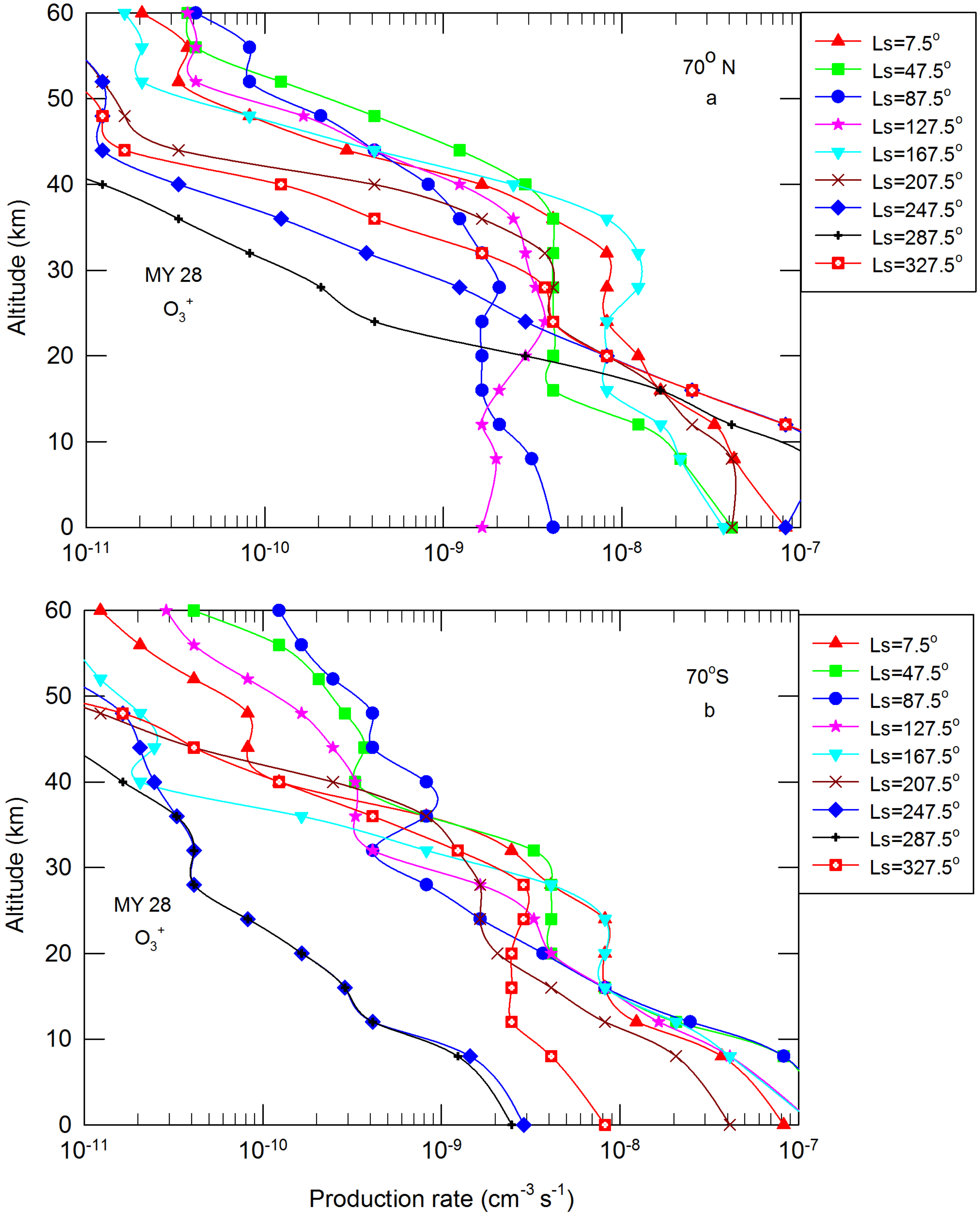

This article is protected by copyright. All rights reserved.